Mining, Metallurgy & Exploration (2021) 38:187–201
https://doi.org/10.1007/s42461-020-00310-w

Kinetics of Atmospheric Leaching from a Brazilian Nickel Laterite Ore Allied to Redox Potential Control

A. L. A. Santos[1] · E. M. A. Becheleni[2] · P. R. M. Viana[1] · R. M. Papini[1] · F. P. C. Silvas[3] · S. D. F. Rocha[1]

Received: 27 May 2020 / Accepted: 11 September 2020 / Published online: 7 October 2020

Abstract

The kinetics of atmospheric sulfuric acid leaching from a Brazilian nickel laterite ore was assessed using distinct reducing agents and ore mineralogy. This transitional ore contains 1.63% Ni distributed as 1.27% in coarse size (− 500 + 150 μm), mainly as silicates (lizardite and chlorite — 28.6%), and 2.06% in the fines fraction (− 75 μm), mainly as iron oxy-hydroxides (goethite and hematite — 49%). The effects of temperature, acid concentration, reducing reagent type, and concentration were evaluated. The − 75 μm fraction limited the leaching efficiency and the use of reducing media with thiosulfate improved leaching and Ni-Fe selectivity. However, at constant E_h of 626–743 mV and a pH range between 0.2 and 1.1, no substantial rise in metals extraction, except for Co and Mn, has been observed. In order to determine the process control at 95 °C, two regions in the extraction curves were used in combination with the shrinking core model. Control by porous diffusion was observed and the kinetic constant was found to be in the order $k_{Fe}<k_{Ni}<k_{Mn}<k_{Co}<k_{Mg}$ for atmospheric leaching without E_h control. In reducing media for the first 15 min of leaching, the kinetic constant was found to be $k_{Fe}<k_{Ni}<k_{Mg}\cong k_{Co}<k_{Mn}$ as derived from Ni disseminated into iron oxides structures.

Keywords Laterite ore characterization · Transitional Ni-laterite · Thiosulfate · Sulfur salts agents · Reducing leaching condition · Kinetic mechanism

1 Introduction

Accounting for approximately 60% of world nickel resources, nickel laterite ores contribute up to 50% of the annual production of nickel [1]. Although nickel can also be found in sulfide deposits and processed by conventional methods of mineral processing, laterite ores have become an additional source due to increasing demand [2]. Because of its growing applications, the nickel price has been rising since the second quarter of 2016, when the lowest average price (9549 \$ t^{-1}) was registered by the London Metal Exchange [1].

Formed by intense weathering processes influenced by topography, drainage, and other hydrogeological factors in mafic and ultramafic bedrocks, the laterite profile of nickel often exhibits high variability in composition and characteristics. In these deposits, Ni occurs finely disseminated either within the iron oxides (via substitution of Fe in their crystalline structures) or incorporated into magnesium silicates structures instead of being present as a separate mineral phase [3]. Therefore, in these cases, the Ni grade cannot be increased by conventional concentration methods of mineral processing such as flotation, thus requiring direct hydrometallurgical processes [4–6].

Hydrometallurgical processing is the most appropriate approach for this type of ore because the mineral structure needs to be broken up to extract and further recover the nickel [7, 8]. This requirement explains the development of new technologies, including high-pressure acid leaching (HPAL) and atmospheric acid leaching, both of which contribute to making the laterite process cost-effective. In particular, atmospheric acid leaching at low temperatures and in open vessel avoids the needs of expensive HPAL autoclaves. However, key issues

✉ A. L. A. Santos
asantos@demin.ufmg.br

✉ S. D. F. Rocha
sdrocha@demin.ufmg.br

[1] Departament of Mining Engineering, Universidade Federal de Minas Gerais, Belo Horizonte, MG 31270-901, Brazil

[2] Institute of Engineering, Science and Technology, Universidade Federal dos Vales do Jequitinhonha e Mucuri, Janaúba, MG 39447-790, Brazil

[3] Vale Institute of Technology, Ouro Preto, MG 35400-000, Brazil

arise, such as the kinetics of nickel dissolution and the subsequent step for liquor purification [9].

Recent studies on nickel atmospheric acid leaching have shown dependence on many variables such as temperature, acid concentration, solid-liquid ratio, and stirring rate [5, 10–17]. In the case of nickel laterite ores, variable recoveries, depending on ore properties and leaching conditions, have been observed. Nickel recoveries from 76 to 95% have been reported at 95 °C, high acid concentrations (up to 8 mol L^{-1}), and prolonged leaching time (over 4 h) [5, 10, 12, 17].

Atmospheric sulfuric acid leaching is not selective for Ni or Co because common gangue metals such as Fe, Mg, and Mn are simultaneously dissolved. McDonald and Whittington proposed strategies at improving the nickel laterite extraction in less severe conditions [9]. These included leaching under a controlled redox potential of the pulp by the addition of inorganic reducing agents such as sulfur dioxide and cuprous ions [13], sodium sulfite [18], and sodium thiosulfate [14]. In the study of Li et al., the use of thiosulfate was selective for Co giving extractions of 91% Co, 22% Ni, and 10% Fe in 5 min at 90 °C, using 10 g L^{-1} of sodium thiosulfate, 8 wt.% (0.9 mol L^{-1}) of H_2SO_4, and a 10:1 of liquid-solid ratio [14].

This study seeks to (i) evaluate the kinetics of leaching a Brazilian nickel laterite ore with sulfuric acid under atmospheric conditions to focus on the impact of the use of distinct reducing agents with an emphasis on thiosulfate and (ii) to determine how the specific characteristics of the ore affect the process efficiency.

2 Materials and Methods

2.1 Ore Sampling and Characterization

The laterite ore was received in quantities of 5 kg from the mining operation in northern Brazil. After homogenization, it was sieved and dried at 60 °C for 24 h. Samples were then subjected to physical, chemical, and mineralogical characterization. The leaching experiments were carried out on samples with three distinct particle sizes (− 500 + 150 μm, − 150 + 75 μm, and − 75 μm) obtained by wet sieving and subsequent drying.

Particle size distribution was obtained by sieving and cyclosizer, the specific surface area was determined based in Brunauer-Emmett-Teller theory (BET) (Quantachrome NOVA 1200e), and real density was measured through pycnometer. Water content as the humidity was determined in an oven at 120 °C (Fanem Orion 515) and loss on ignition (LOI) was determined in a furnace at 1100 °C (furnace) (TradeLAB Ambiental TLA200F).

Dispersive X-ray spectroscopy (EDS) (Thermo Noran 6714A-1SUS-SN) and atomic absorption spectrometry (AAS) (GBC, model Avanta) were used to measure Fe, Ni, Mg, Mn, and Co grades while inductively coupled plasma optical emission spectroscopy (ICP-OES) (Varian Vista Pro) was used for Si analyses.

An X-ray diffractometer (Panalytical X'Pert Powder, controller PW3710/31, generator PW1830/40, and detector 3020/00) coupled with Rietveld refinement was used for identification and quantification of mineral phases. Particle morphology was observed with the use of a scanning electron microscope (SEM) (JEOL LSM 6360LV and Quanta 200 FEI).

2.2 Screening Leaching Experiments

Screening tests were carried out to identify preliminary atmospheric acid leaching experimental conditions such as temperature, acid concentration, solid-liquid ratio, and stirring rate. The experiments were set up in a 1 L glass reactor equipped with a Teflon impeller and a vapor reflux condenser above the reactor to keep the solid-liquid ratio constant. The temperature was kept constant with a thermostat electrical heating (± 0.1 °C).

A sulfuric acid solution (0.9 mol L^{-1}) was added into the reactor and heated until the setup temperature (65 or 95 °C) at a constant stirring rate (200 or 400 rpm). After achieving the desired temperature, a suitable mass of ore (− 500 + 150 μm, − 150 + 75 μm, or − 75 μm) was added into the system to obtain a pulp density of 20%. Samples were then collected after 15, 30, 60, 120, 180, 240, 300, and 360 min of leaching, vacuum filtered in an 8 μm paper filter, followed by filtration in fiberglass with a porosity of 1 μm, and subsequently subjected to chemical analysis.

2.3 Atmospheric Acid Leaching and Reducing Atmospheric acid Leaching

Leaching with and without reducing agents (RAAL and AAL) was carried out in the same system as described in Section 2.2. Acid concentration, temperature, and the use of reducing agents were evaluated, as well as the concentration of reducing agent. Moreover, the effect of leaching solution restoration — the addition of a fresh leaching solution as the same volume as the liquor sampled — for size fractions smaller than 75 μm was also evaluated. A stirring rate of 400 rpm was adopted for all experiments.

The atmospheric acid leaching (AAL) experiments were carried out at 95 °C with a solid-liquid ratio of 15% and an initial H_2SO_4 concentration of 2 mol L^{-1} with solution restoration of H_2SO_4 2 mol L^{-1}. Samples were collected after 30, 60, 120, 180, 240, 300, and 360 min for further analysis.

To assess the most efficient reducing agent for reducing atmospheric acid leaching (RAAL), sulfite (30 g L^{-1}), dithionite (30 g L^{-1}), metabisulfite (30 g L^{-1}), and thiosulfate

(10 g L^{-1}) sodium salts were evaluated in duplicates at 95 °C using a solid-liquid ratio of 15% and 0.9 mol L^{-1} H_2SO_4 for 360 min. Sodium thiosulfate was selected as the best reducing agent and its initial concentration was also evaluated in the range of 10, 20, and 30 g L^{-1} ($S_2O_3^{2-}$) at 95 °C using a solid-liquid ratio of 15% and 2 mol L^{-1} H_2SO_4.

The evaluation of a constant pH and E_h conditions on leaching experiments was carried out with the restoration of the leaching solution. The same experimental conditions were used (temperature of 95 °C, solid-liquid ratio of 15%, and an initial H_2SO_4 concentration of 2 mol L^{-1}). The initial thiosulfate concentration was 10 g L^{-1} and the solution restoration contained H_2SO_4 4 mol L and thiosulfate 113 g L^{-1} of thiosulfate (250 g L^{-1} of $Na_2S_2O_3{\cdot}5H_2O$) (RAAL). Sampling was carried out after 30, 60, 120, 180, 240, 300, and 360 min for subsequent chemical analysis.

Subsequent experiments at E_h and pH constant leaching conditions were carried out in triplicate using H_2SO_4 concentrations of 0.7, 1.0, or 2.0 mol L^{-1}, temperatures of 65 or 95 °C, and a solid-liquid ratio of 15% with the restoration of the leaching solution. A 10 mL sample of liquor was collected after 5, 15, 30, 60, and 120 min, filtered and diluted adequately for further chemical analysis.

In the case of the AAL, the leaching solution restoration was made with 10 mL of H_2SO_4 concentrations of 0.7, 1.0, or 2.0 mol L^{-1}. For AAL experiments, the reducing agent was added to the pulp and the restoration of the leaching solution kept the leaching conditions constant by adding 5 mL of acid with double the initial concentration (1.4, 2.0, and 4.0 mol L^{-1}) and 5 mL of 113 g L^{-1} thiosulfate. The solid obtained by samples filtration (cake) was also restituted to the leaching reactor.

2.4 Kinetic of Leaching

The kinetic analysis was carried out using the shrinking core model [19]. The controlling step of leaching may be coherent with only one model or even a combination of models. Assuming that volume diffusion (VD), porous layer diffusion (PLD), and chemical reaction (CR) control the leaching reaction, the respective kinetic models (Eqs. 1, 2, and 3) were used to evaluate the experimental results.

$$x = k_{VD} \cdot t \tag{1}$$

$$1-3(1-x)^{\frac{2}{3}} + 2(1-x) = k_{PL} \cdot t \tag{2}$$

$$1-(1-x)^{\frac{1}{3}} = k_{CR} \cdot t \tag{3}$$

where x is the fraction leached or metal extracted, k is the apparent rate constant, and t is the reaction time.

3 Results and Discussion

3.1 Ore Sampling and Characterization

The particle size distribution of the ore is shown in Fig. 1. Particles − 75 μm represented more than 50% of the ore and 44% of particles were found to be smaller than 38 μm. Furthermore, greater than 20% were found to be very tiny particles (− 10 μm) as expected for laterite ores, suggesting that the material under investigation is a transitional saprolitic to limonitic ore. These results are in good agreement with those reported by the literature [12, 18, 20].

Commonly, physical characteristics of laterite ores have not been presented in the literature, making it difficult to correlate the leaching performance with each type of ore studied. Fan and Gerson reported that a limonitic portion is usually concentrated in tiny particle fractions (d_{80} = 30 μm), while the saprolitic type predominates in larger particles (d_{80} = 200 μm) [20]. Recent work by MacCarthy et al. characterized an ore with a transitional state between saprolite and limonite where many particles in the fine size range were presented (d_{90} of 630 μm and d_{50} of 53 μm) [11].

The specific surface area (SSA_{BET}) for distinct particle size fractions is presented in Table 1, exhibiting the usual inverse relationship between particle size and surface area. Pore sizes were observed to be constant within the whole particle size ranges investigated. A real density of (2.9 ± 0.1) g cm^{-3}, moisture content of 7.2 ± 0.2%, and a LOI of 8.1 ± 0.3% were determined for this ore. The water content found for Brazilian nickel laterite ore was in the range of 8–45%, established by literature as moisture and chemically combined water in hydrate minerals [21, 22] .

According to the chemical analysis (Table 2), Fe is concentrated in the fine fraction and Si is mostly present in the coarser fraction. Co and Mn do not present any accumulation profile in a specific range of particle size. Although Mg is not preferentially present in any fraction, the Si content is higher in the coarser fraction, which infers that Mg-minerals (e.g., Mg-silicates) may be concentrated in this fraction (Table 3).

As expected, any nickel-specific mineral phase was found in the ore (Table 3). Quartz, chlorite, hematite, goethite, and magnetite/maghemite were identified as major phases in the three distinct particle size ranges (− 500 + 150 μm, − 150 + 75 μm, and − 75 μm) and in the head sample ore. This is in good agreement with nickel laterite ores observed from Indonesia, Iran, Australia, New Caledonia, China, and Turkey [3, 5, 12, 15, 22, 23]. Amphibole was also identified in the − 150 + 75 μm fraction. Some other mineral phases, such as lizardite and chromite, were in minimal proportion depending on the sample.

From Table 3, it can be observed that Mg-minerals such as lizardite and chlorite predominate in the coarser

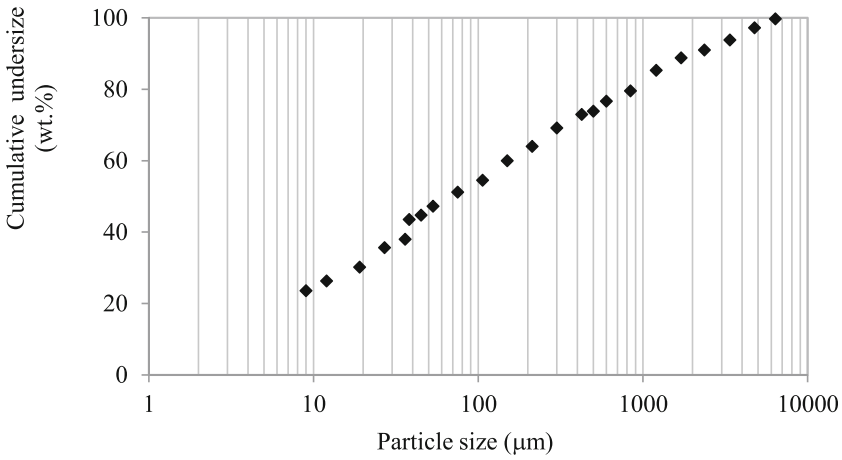

Fig. 1 Particle size distribution of the nickel laterite ore

fraction (− 500 + 150 μm, up to 28.7%). In contrast, the iron oxy-hydroxide phases are concentrated in the smaller fraction (− 75 μm, up to 57%) with goethite dominating. Mg-minerals (chlorite and lizardite) represented 26.8% of the head sample ore and iron oxy-hydroxide phases comprised 40% with goethite being dominant.

Based on SEM/EDS analysis (Fig. 2), Ni appears to be associated with the oxy-hydroxide and silicate phases in a distinct extent as highlighted in the literature [23]. Many particles with morphologies such as lamellar, striated, platy, and globular forms were observed as well as mixed particles with tiny sizes. Amphibole particles were identified by stretch marks on their surfaces in a fibrous structure. The calcium detected by chemical analysis could indicate the presence of tremolite, but this mineral was found to be rare in the whole sample.

Previous SEM/EDS analysis of 24 distinct samples of the ore fractions are excluded from this paper. However, the observed feature revealed an accumulation of Fe and Ni in small particles (− 75 μm) while Mg does not show a concentration tendency in any specific size. This is further confirmed by the quantitative chemical analysis presented in Table 2. The Ni contained in this ore is mainly associated with a mineral, or it is strongly associated with goethite by substitution of Fe into its crystalline structure [24–26] or is incorporated into the magnesium silicates structures. Such behavior is attributed to the aggressive weathering effect experienced by the rock formation of the ore [7].

3.2 Screening Leaching Experiments

Figure 3 presents Ni and Fe extraction at different agitation rates. It is possible to verify that even after 360 min, the extraction of Fe did not stabilize, while a trend to equilibrium was observed for Ni extraction after 300 min. In contrast to Ni, Fe extraction was not affected by the particle size, which has been attributed to the two different categories of mineralogy present. Namely, Ni-bearing magnesium silicates predominate in the − 500 + 150 μm sample and iron oxy-hydroxides are the main present as goethite in the − 75 μm fraction.

The extraction was not improved when the stirring rate was increased from 200 to 400 rpm, thus indicating that proper mixing was obtained even at a lower stirring rate. Mohammadreza et al. and MacCarthy et al. evaluated the effect of stirring rate with no observation of significant impact on the extraction of metals in the range of 500 to 1000 rpm [5, 10]. Furthermore, it indicated that the leaching process is not controlled by mass transfer nor volume diffusion.

As indicated in Fig. 3, the extraction of Fe reached levels from 7.3 to 8.3% for all conditions, in 360 min. This corresponds to Fe concentrations in the liquor of 4.2 g L^{-1} and 7.0 g L^{-1}, respectively. However, unexpectedly, despite the low ore grade, nickel extraction from coarser particles was higher (53%) than for smaller particles (28%). The final liquor concentrations were the same for both samples (1.6 g L^{-1}). This behavior was attributed to the fact that in the coarser fraction, nickel is mainly associated with silicates, while in

Table 1 Specific surface area and porosity of nickel laterite ore

Particles size range	SSA_{BET} (m^2 g^{-1})	Porosity	
		Pores volume (cm^3 g^{-1})	Average pores size (nm)
− 500 + 150 μm	42	0.081	8.5
− 150 + 75 μm	46	0.066	6.8
− 75 μm	72	0.130	8.3

Table 2 Quantitative chemical analysis of nickel laterite ore

Element grade (%)	Sample composition (%)			
	Head sample ore	− 500 + 150 μm	− 150 + 75 μm	− 75 μm
Ni	1.63 ± 0.009	1.27 ± 0.01	1.48 ± 0.04	2.06 ± 0.02
Fe	29.2 ± 0.06	22.8 ± 0.1	24.7 ± 0.1	35.6 ± 0.1
Si	16.8 ± 0.02	19.3 ± 0.03	16.98 ± 0.04	10.76 ± 0.04
Mg	3.61 ± 0.02	3.64 ± 0.02	3.49 ± 0.03	3.40 ± 0.05
Co	0.103 ± 0.05	0.118 ± 0.001	0.114 ± 0.007	0.095 ± 0.002
Mn	0.525 ± 0.02	0.467 ± 0.005	0.460 ± 0.006	0.401 ± 0.004

the fine particles, the association with iron oxy-hydroxide is predominant.

The higher extraction of Ni in coarser fraction also implies that Ni-bearing magnesium silicates are easily leachable than other minerals such as goethite. This agrees with previous studies that have reported that nickel was more readily leached from clay-like minerals (silicate ores) than oxy-hydroxide ores (limonite, goethite) [8, 23, 27]. This effect reflects in higher Fe/Ni molar ratios of the liquors obtained from small particles, thus indicating that there is a restrictive fraction that affects the leaching process, thereafter called limiting fraction which is studied in the present work.

The increase in temperature from 65 to 95 °C improved the extraction for both metals (Fe and Ni) in all particle size ranges (Fig. 4). However, the effect was more pronounced for the – 150 + 75 μm fraction where Ni and Fe extraction were increased from 31 to 43% and 7.6 to 10%, respectively. The effect of temperature has also been observed in the literature with a concern that an increase in temperature favors the extraction of Ni and other elements (Fe, Mn, Co, and Mg) due to its influence on chemical reaction kinetics [5, 10, 11, 14, 16, 17].

The fraction − 75 μm contains 64% of the entire Ni present in the ore, and it is mainly composed of iron oxy-hydroxides, especially goethite, which is not suited to leaching and requires a more extreme condition for efficient recovery (acid dosages up to 4900 kg t^{-1} dry ore). In this study, this fraction is assigned as the limiting fraction of leaching.

Due to the knowledge of restrictive and limiting leaching fraction, to further understand how this specific mineral association affects the whole ore leaching, a detailed study of the − 75 μm fraction was undertaken, keeping the stirring rate at 400 rpm. The solid-liquid ratio was changed to 15% because a visual increase in viscosity of the slurry at 20% solids was observed. Panda et al. and Li et al. indicated that a high solids content could hamper the ionic mobility, thus decreasing leaching efficiency, but in their work, viscosity was not measured [12, 14].

Table 3 Quantitative mineralogical composition of nickel laterite ore by Rietveld analysis

Mineral phase		Sample composition (%)		
		Head sample ore	− 500 + 150 μm	− 75 μm
Silicates	Quartz	27.3	46.7	21.0
	Chlorite	21.8	15.3	19.9
	Lizardite	4.8	13.4	2.0
Oxides	Goethite	28.1	13.2	41.7
	Hematite	7.2	2.2	7.3
	Magnetite	4.8	2.1	8.6
	Cromite	6.0	8.2	0.5

3.3 AAL and RAAL study

Sulfur dioxide has been widely used as a reducing agent to improve metal extraction [28, 29]. This agent has advantages such as direct reduction of Fe, Mn, and Co oxides, as well as producing Fe^{2+} ions that act as an intermediary species for leaching of Mn and Co [28]. The downside of using sulfur dioxide as a reducing agent for metal extraction relates to environmental health hazards as well as lower mass transfer efficiencies, all of which have stimulated the alternative use of sodium-sulfur salts [14, 18].

Figure 5 shows the extraction of Ni and Fe in the presence of reductant agents and also the molar ratio of Fe/Ni extracted during the entire process. As presented in Fig. 5a, the extraction of Ni benefits from the presence of diverse reducing agents, reaching up to 57% (thiosulfate) while 35% was found in AAL. In contrast, Fe extraction showed higher values only during the initial period (120 min), where its extraction reaches 15–20% in RAAL and 8–13% in AAL. However, by the end of the process (360 min), the metal extraction was close to that of atmospheric leaching (17%), which is of great interest to improve Ni/Fe selectivity. The redox potential (E_h) was maintained between 610 and 700 mV, lower than the 710 to 770 mV, as described by Fan and Gerson for saprolitic ores [20].

Under reducing conditions, the leaching kinetics were faster than in atmospheric leaching, and stable extractions were reached

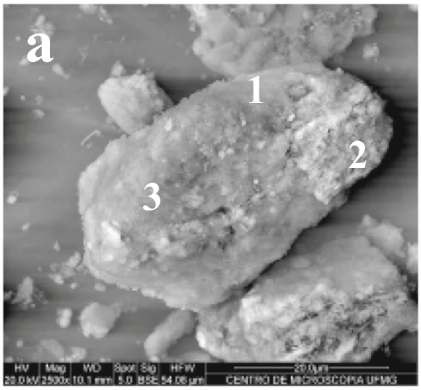

a			
EDS	1	2	3
High	Si, Fe	Fe	Si, Fe
Medium	Al, Mg	Al, Mg, Si	Al
Low	Ni	Ni	Ni, Mg
Traces	Co, Cr, Ti	Cr, Co	Cr, Co Ca, Ti

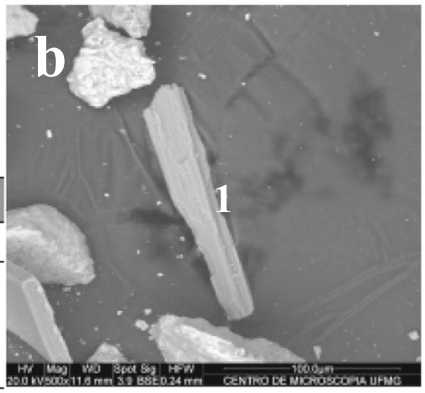

b	
EDS	1
High	Si, Mg
Medium	Ca
Low	Al, Fe
Trace	Ni

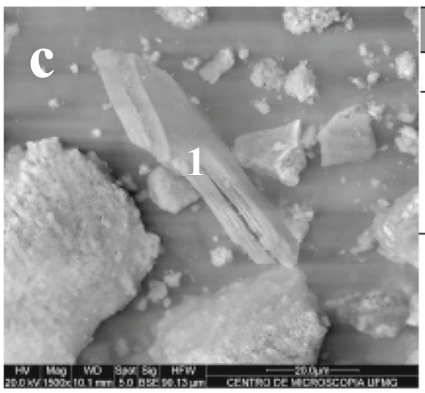

c	
EDS	1
High	Si, Mg
Medium	Al, Fe
Low	Ni
Trace	Co, Cr, Cl, Ti

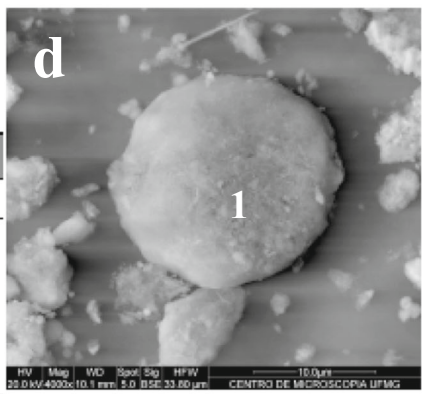

d	
EDS	1
High	Fe
Medium	Al, Si
Low	Ni, Mg
Trace	Co, Cr, Ca, Ti

Fig. 2 Backscattered electron images from SEM/EDS analysis of mixed particles (**a**), amphibole (**b**), chlorite (**c**), and iron oxide (**d**)

within 120 min. This time was defined as the period to carry out future tests. For this step, from Fig. 5b, the leaching of nickel occurred linearly in association with the iron leaching behavior derived from their association revealed by chemical and mineralogical analysis.

The trend in line of Fe/Ni molar ratio changed and shifted, indicating that many of the reducing agents improved the selectivity of the process (except for the dithionite). Dithionite increased Ni and Fe extraction in the same ratio observed for the system without reducing agents (Fe/Ni ≅ 6.2) as it follows the same straight line as that of AAL (Fig. 5b). This indicates that this reactant acts on the same Ni-Fe phase. Finally, it is worth noting that thiosulfate was the most effective reducing extractant if it is considered that Ni must be selectively leached. Since, for the same Ni concentration, the Fe/Ni ratio both for RAAL using dithionite and AAL are aligned in the same straight line, which indicates that dithionite presents lower selectivity, due to extra Fe leaching of 32% in comparison to the other reductant agents selective for Ni.

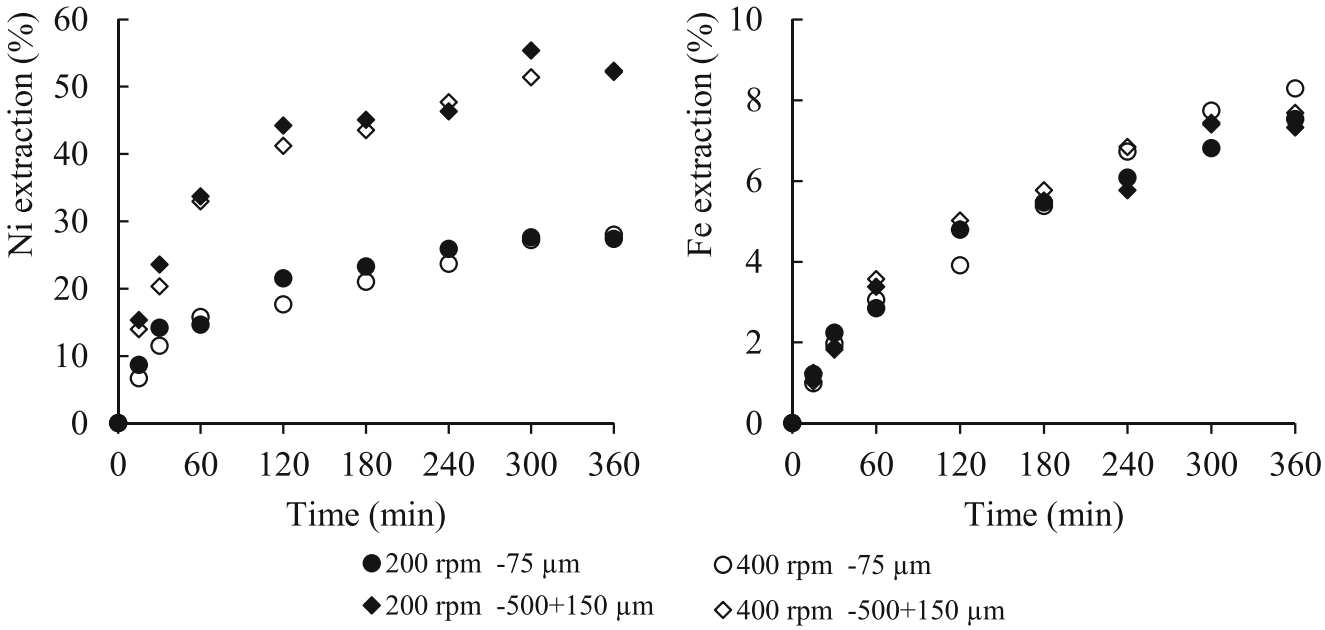

Fig. 3 Ni and Fe extraction evolution during leaching tests for distinct stirring rates and particle size ranges. Temperature: 65 °C. Solid-liquid ratio: 20%. H_2SO_4 0.9 mol L^{-1}

Hence, this reagent was not selected for the subsequent experiments.

The acid leaching mechanism of nickel laterite is widely discussed in the literature. The dissolution of goethite was found to occur on singly coordinate hydroxyl groups which would be easier to remove than doubly or triply coordinated hydroxyl groups [30]. Some authors suggest that counter ions of acid also support complexation at the goethite surface improving its dissolution [31, 32]. Other ones indicate that the substitution of Fe into crystalline structures plays an important role in the leaching, being Al and Cr-goethite harder to extract than Ni, Co, or Mg-containing goethite [33].

The acid mechanism of oxide dissolution involves key steps summarized by Eqs. 4 and 5 (surface protonation), and Eq. 6 (desorption) [9]:

$$\vdash_s OFe^{III}O + H^+ \rightleftharpoons \vdash_s OFe^{III}OH \quad (4)$$

$$\vdash_s OFe^{III}OH + H^+ \rightleftharpoons \vdash_s OFe^{III} + H_2O \quad (5)$$

$$\vdash_s OFe^{III}OH + H^+ \rightleftharpoons \vdash_s OH + (Fe^{III}O)^{2+} \quad (6)$$

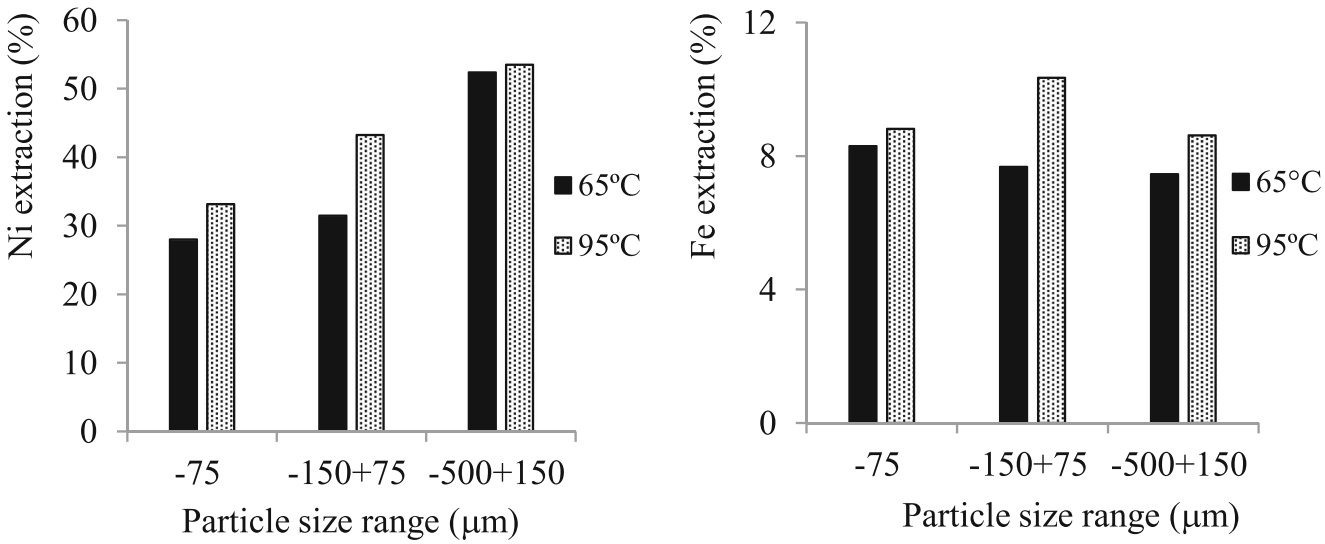

Fig. 4 Ni and Fe extraction after 360 min of leaching at 65 and 95 °C. Solid-liquid ratio: 20%. H_2SO_4: 0.9 mol L^{-1}. Stirring rate: 400 rpm

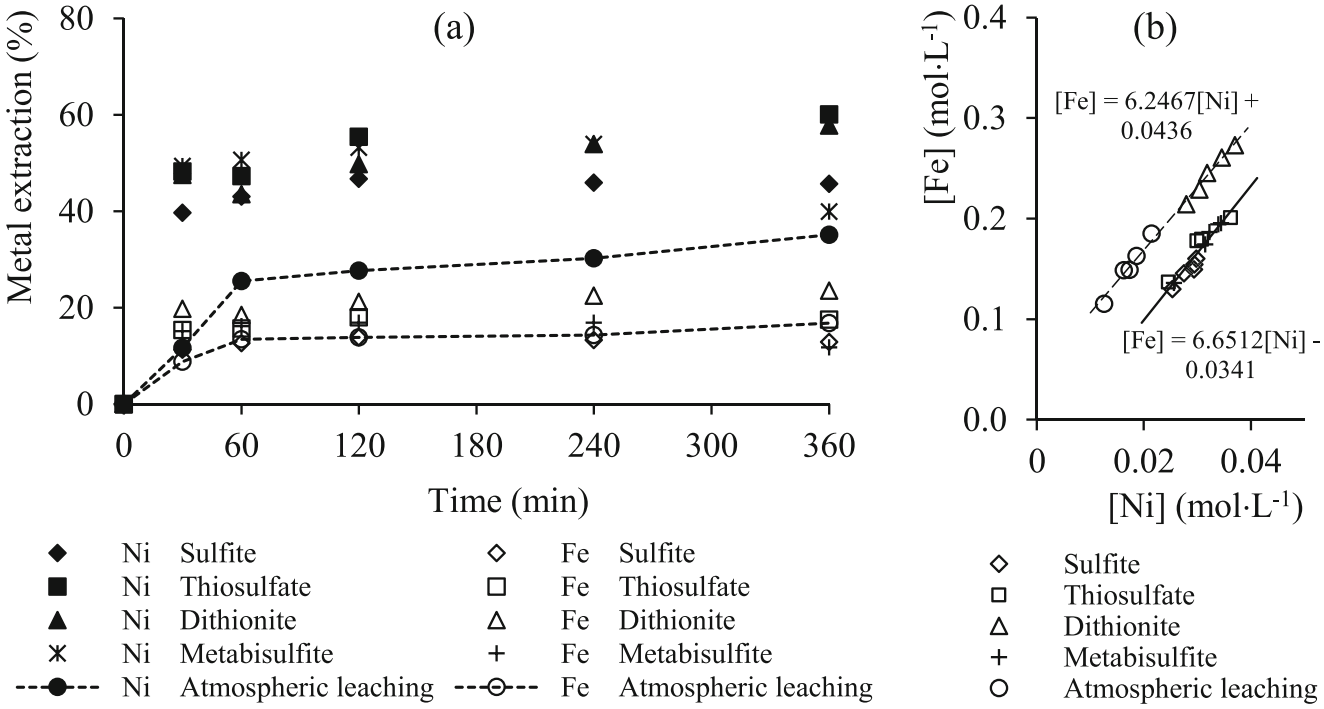

Fig. 5 **a** Extraction for Ni and Fe in the absence (AAL) and in the presence (RAAL) of reducing agents and **b** Fe/Ni molar ratio. Temperature: 95 °C. Solid-liquid ratio: 15%. Particle size fraction: − 75 μm. H_2SO_4: 0.9 mol L^{-1}. Sulfite, Dithionite, and Metabisulfite: 30 g L^{-1}. Thiosulfate: 10 g L^{-1}. Stirring rate: 400 rpm

On the other hand, while extraction of Ni from goethite needs complete dissolution of the grain [34], Ni extraction from serpentine and chlorite groups did not require its complete dissolution [9, 35]. The mechanism of dissolution of Ni from phyllosilicate minerals involves the removal of hydroxyl bonds from the octahedral brucite layer and the tetrahedral silica layers are removed too. This weakens Mg–O bond and releases Ni and Mn to the liquor. In contrast, Si-O bonds remain unaffected in the silicate layer [35].

The reducing leaching mechanism could be slightly distinct from a simple acid attack. In the presence of reductant agents such as sulfite, thiosulfate, and dithionite, the reaction mechanism is related to the generation of soluble sulfur dioxide ($SO_{2(aq)}$) due to hydrolysis or deprotonation, according to Eqs. 7–10, which enables electron transfer on goethite surface [14, 18, 29, 36]:

$$SO_3^{2-} + H^+ \rightleftharpoons HSO_3^- + H^+ \rightleftharpoons SO_{2(aq)} + H_2 \quad (7)$$

$$S_2O_3^{2-} + 2H^+ \rightleftharpoons SO_{2(aq)} + S_{(s)} + H_2O \quad (8)$$

$$S_2O_3^{2-} + H^+ \rightleftharpoons S_{(s)} + HSO_3^- \quad (9)$$

$$2S_2O_4^{2-} + H_2O \rightleftharpoons S_2O_3^{2-} + 2HSO_3^- \quad (10)$$

Once the sulfur dioxide is generated, an electrochemical reaction (Eqs. 11–14) occurs in the surface of goethite, reducing Fe^{3+} to Fe^{2+} and oxidizing SO_2 to SO_4^{2-} [9, 14]. Thus the Fe^{2+} is released to the solution as $(FeOH)^+$. These reactions are simplified in the Eqs. 13–14 [14].

$$\vdash_s OFe^{III}OH + 2H_2O + SO_{2(aq)} \rightleftharpoons \vdash_s OFe^{II}OH + SO_4^{2-} + 4H^+ \quad (11)$$

$$\vdash_s OFe^{II}OH + H^+ \rightleftharpoons \vdash_s OH + (Fe^{II}OH)^+ \quad (12)$$

$$2FeOOH_{(s)} + 2H^+ + SO_{2(aq)} \rightleftharpoons 2Fe^{2+} + SO_4^{2-} + 2H_2O \quad (13)$$

$$4FeOOH_{(s)} + 8H^+ + S_{(s)} \rightleftharpoons 4Fe^{2+} + SO_{2(aq)} + 6H_2O \quad (14)$$

It is worthy to note, as stated by Li et al., that the presence of hydrogen ion and thiosulfate is a key factor to increase Fe and Ni extraction, since Ni is inside the crystalline structure of goethite [14]. This justifies the fact that the leaching of Ni was favored due to the presence of a reductant agent (Fig. 5a).

3.3.1 The Effect of Reducing Agent Concentration

Figure 6 presents the effect of 10, 20, and 30 g L^{-1} of thiosulfate on Ni, Fe, Mg, Co, and Mn extractions. A

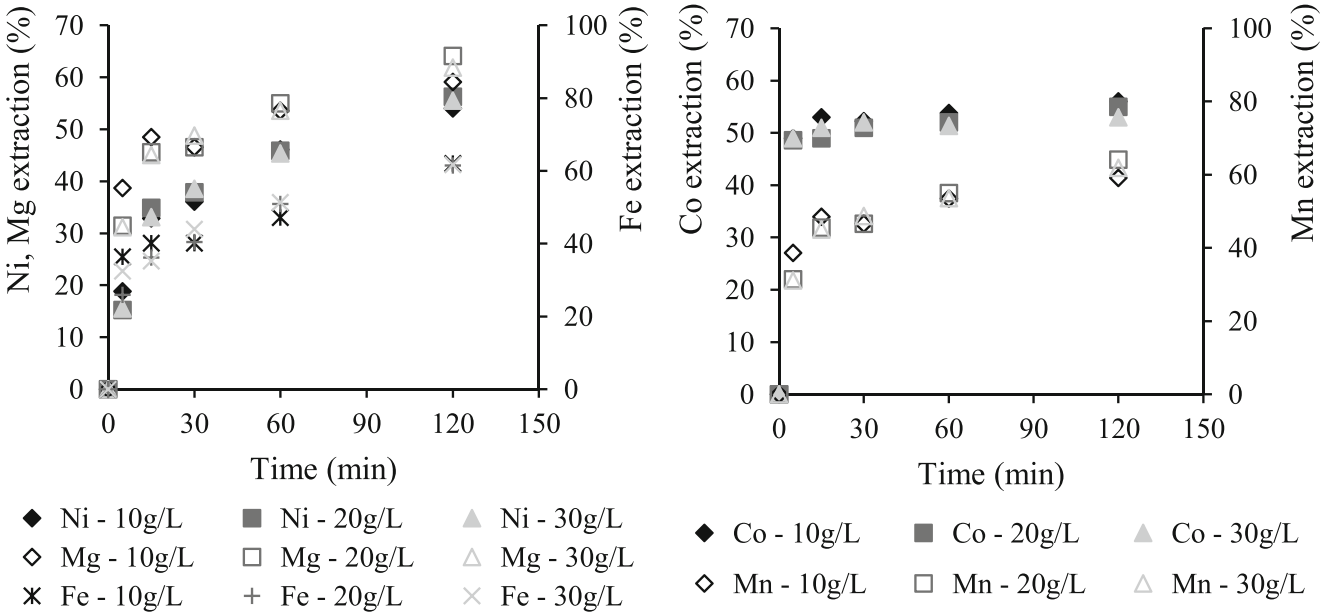

Fig. 6 Ni, Fe, Mg, Co, and Mn extraction at different concentrations of thiosulfate for distinct concentrations of thiosulfate. Temperature: 95 °C. Solid-liquid ratio: 15%. Particle size fraction: − 75 μm. H_2SO_4: 2 mol L^{-1}. Stirring rate: 400 rpm

redox potential (E_h) of 670, 650, and 640 mV for 10, 20, and 30 g L^{-1} of thiosulfate were measured, respectively. In general, the increase of thiosulfate concentration did not enhance metal extraction. The extraction obtained after 120 min was 55% (Ni), 62% (Mg), 61% (Fe), 53% (Co), and 62% (Mn) at 10 g L^{-1} of thiosulfate and E_h of 670 mV.

This agrees with the literature, which has indicated that increasing the concentration of the reducing agent did not improve the leaching efficiencies [14, 29]. Since the variation on the concentration of the reducing agent did not improve metal extraction, the concentration of thiosulfate was kept at 10 g L^{-1} in the subsequent experiments.

3.3.2 Effect of Restoration of Leaching Agent, Temperature, and Initial Acid Concentration for the Limiting Fraction − 75 μm

Figure 7 presents the evolution of metal extraction with and without the restoration of the leaching solution after sampling. As expected, the extraction of the metals was improved by the

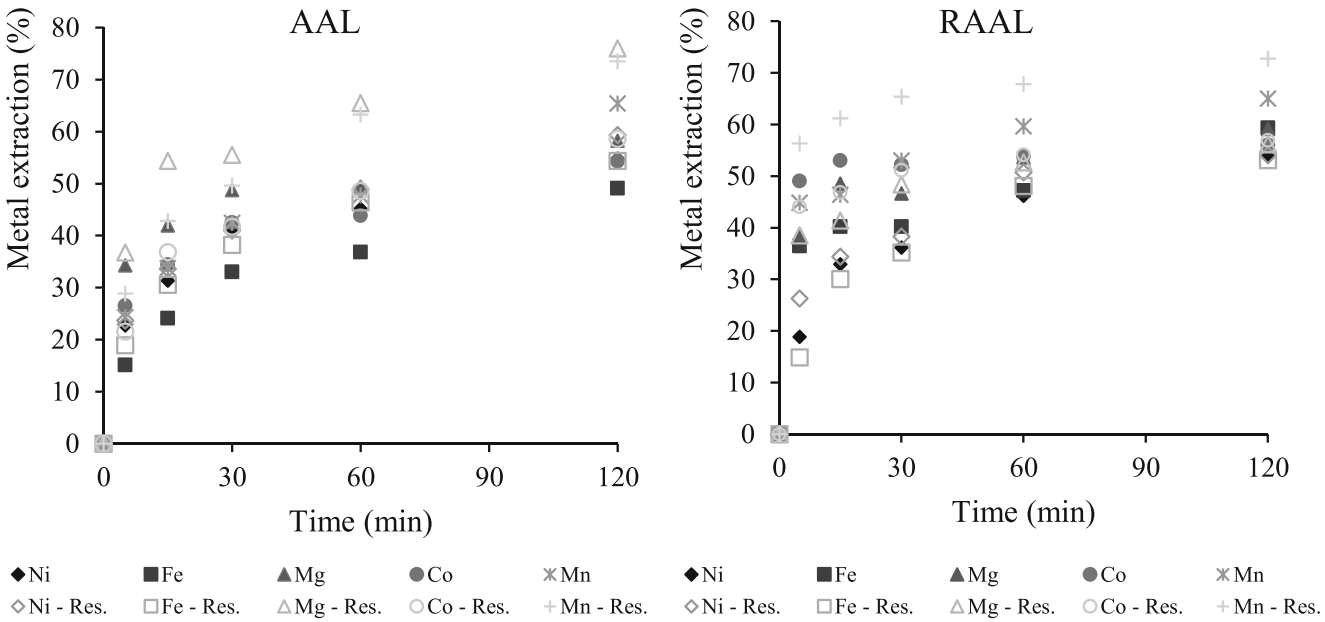

Fig. 7 Ni, Fe, Mg, Co, and Mn extraction from AAL and RAAL with and without restoration of the leaching solution. Temperature: 95 °C. Solid-liquid ratio: 15%. Particle size fraction: − 75 μm. H_2SO_4: 2 mol L^{-1}. Thiosulfate: 10 g L^{-1}. Stirring rate: 400 rpm

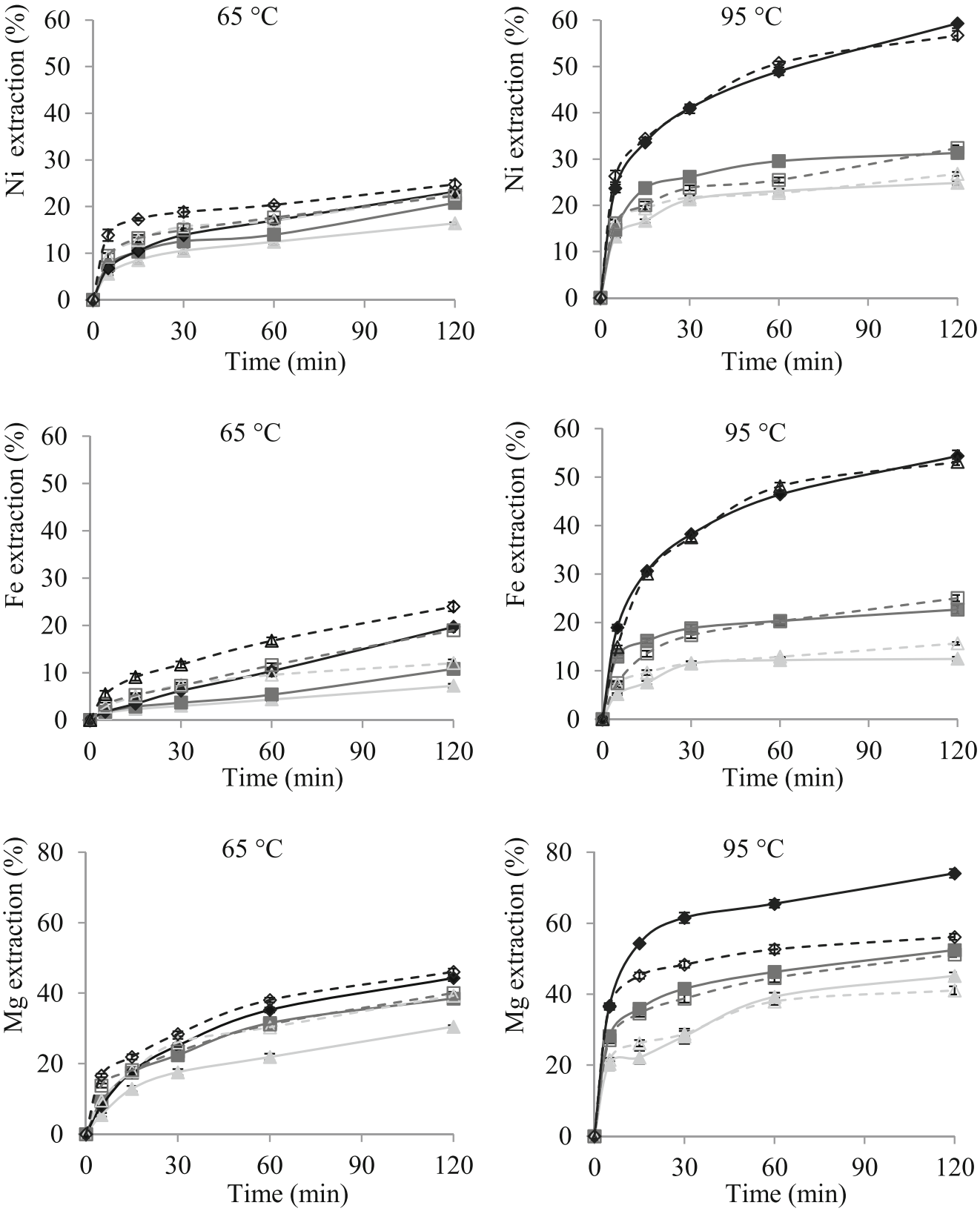

Fig. 8 Ni, Fe, and Mg extractions for AAL (full symbols, continuous lines) and RAAL (empty symbols, dashed lines) at 0.7 mol L^{-1}(white and gray triangle), 1.0 mol L^{-1} (white and black square), and 2.0 mol L^{-1} (white and black diamond) of H_2SO_4 and temperatures of 65 °C (left) and 95 °C (right) with the restoration of the leaching solution. Solid-liquid ratio: 15%. Particle size fraction: − 75 μm. Thiosulfate concentration: 10 g L^{-1}. Stirring rate 400 rpm

restoration of the leaching solution during AAL to different extents. After 120 min of leaching time, the extraction of Ni and Co increased from 54 to 59%, while Fe reached 54% from 49%, and Mg and Mn reached 76% and 74% from 58% and 65%, respectively. However, the same trend was not observed for the RAAL. Ni and Co extractions were similar (54% and 56%, respectively), while Fe and Mg had their extractions decreased from about 60% to 53% (Fe) and 56% (Mg). In contrast, Mn extraction increased from 65 to 73% and the same trend was observed in AAL.

The increase in temperature from 65 to 95 °C generally favored the extraction of metals, with the greatest effect being observed for Ni, Fe, and Mg (Fig. 8) versus that of Mn and Co (Fig. 9). Likewise, Li et al. found a distinct effect of thiosulfate on Ni, Fe and Mg, and Mn and Co extractions due to the rise in temperature from goethite Ni-bearing mineral and manganiferous ore [14]. In the present work, the increase in temperature more than doubled Ni extraction both under RAAL and AAL conditions. It is worth noting that Luo et al. observed a 20% enhancement in Ni extraction from a typical limonitic nickeliferous laterite ore due to an increase in temperature from 30 to 90 °C [16].

In this study, the reducing environment did not display an increase in the extraction of Ni and Fe at the higher temperature of 95 °C. Yet, at the lower temperature of 65 °C, it was possible to get an enhancement of all metal extraction, but not for Mg. Consequently, these results indicate that only the reducing environment (E_h of 626 to 743 mV) at a pH between 0.3 and 1.1 has not been enough to raise the Ni, Fe, or Mg extractions.

Figure 10 presents the E_h and pH areas of AAL and RAAL conditions in a section of Pourbaix diagrams of Fe-H_2O, Ni-H_2O, and S-H_2O systems at 25 °C and 95 °C. These diagrams

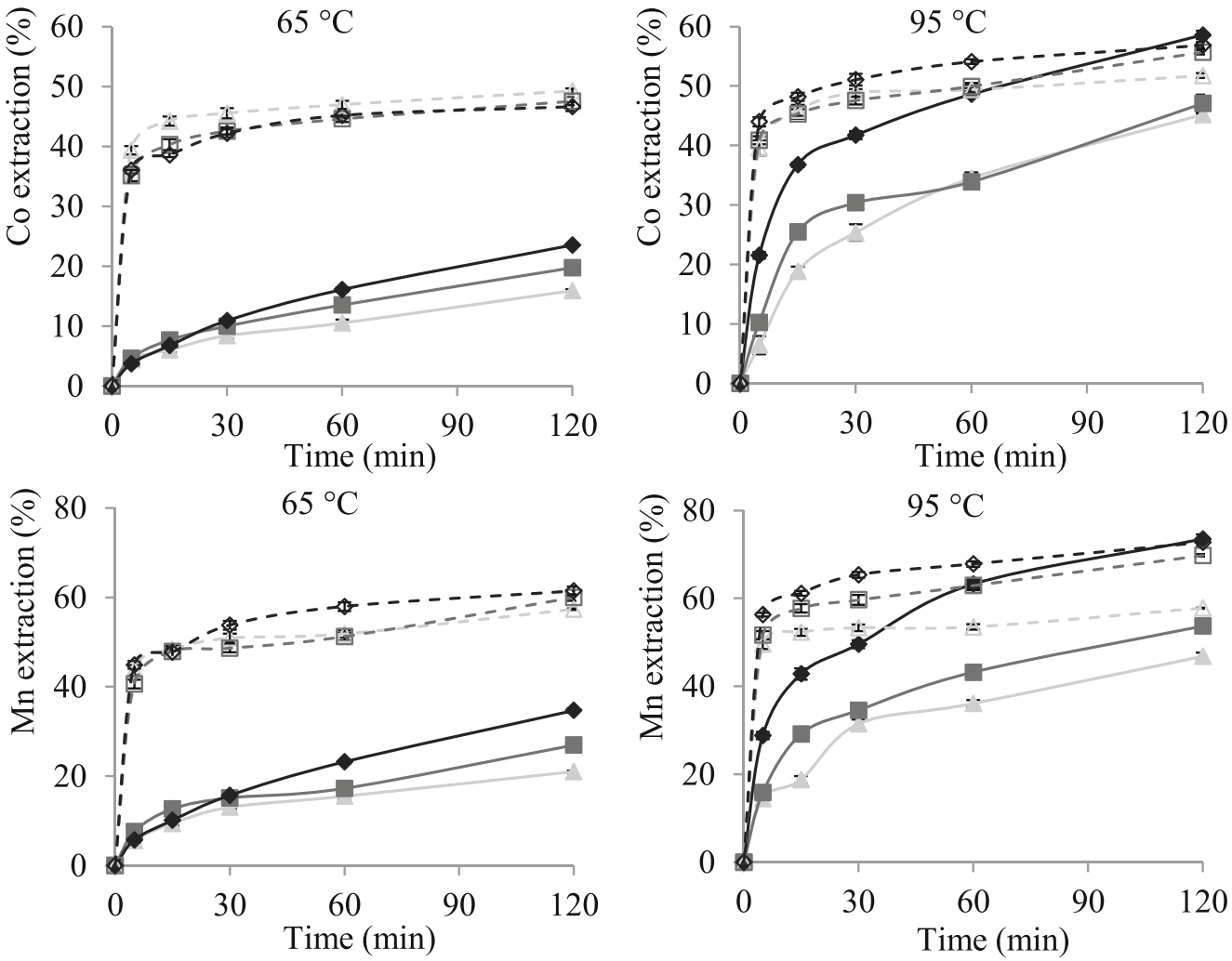

Fig. 9 Co and Mn extraction for AAL (full symbols, continuous lines) and RAAL (empty symbols, dashed lines) at 0.7 mol L^{-1}(white and gray triangle), 1.0 mol L^{-1} (white and black square), and 2.0 mol L^{-1} (white and black diamond) of H_2SO_4, temperatures of 65 °C (left) and 95 °C (right) with the restoration of the leaching solution. Solid-liquid ratio: 15%. Particle size fraction: − 75 μm. Thiosulfate concentration: 10 g L^{-1}. Stirring rate 400 rpm

were made with metals and sulfur molalities from leaching conditions correspond to AAL with 2.0 mol L^{-1} of H_2SO_4 and a 15% solid-liquid ratio. The range of AAL experimental conditions kept in the reactor for initial pH 0.7, 1.0, and 2.0 was, respectively, pH 0.8 ± 0.2 and E_h (944 ± 40) mV, pH 0.7 ± 0.2 and E_h (927 ± 40) mV, and pH 0.3 ± 0.3 and E_h (883 ± 45) mV. The use of thiosulfate promoted a reduction in the range of RAAL experimental conditions in the reactor. These conditions for initial pH of 0.7, 1.0 and 2.0 were, respectively, pH 0.8 ± 0.2 and E_h (658 ± 28) mV, pH 0.7 ± 0.2 and E_h (671±20) mV, and pH 0.4 ± 0.2 and E_h (697 ± 17) mV.

During AAL, the condition in the reactor (E_h versus pH) is located awfully close to the goethite stability region. Thus, the conditions may hinder the leaching of Fe and consequently affects the extraction of Ni due to the Ni-Fe association. At reducing condition (lower E_h), the stability region of soluble Fe species is amplified, hence favoring leaching. Although goethite is unstable under reducing conditions (e.g., RAAL), an increase in Ni leaching was not observed. Additionally, it is worth noting that in the present case, Ni is also associated with silicates that have not shown any effect on leaching efficiency by the presence of thiosulfate.

On the other hand, Co and Mn exhibited distinct behavior in atmospheric and reducing environments. The favored leaching of Mn and Co from pyrolusite (MnO_2), over the Fe dissolution from goethite (FeOOH) in reducing media, has been previously reported [14]. The extraction of Co and Mn in AAL increases from 23 to 58% and 34 to 72%, respectively, by increasing temperature from 65 to 95 °C while using 2.0 mol L^{-1} of H_2SO_4. In contrast, only slight growth in the extraction of Co and Mn from 46 to 61% at 65 °C and 56 to 62% at 95 °C was observed during RAAL with 2.0 mol L^{-1} of H_2SO_4.

Although a substantial increase in Ni, Fe, and Mg extraction in reducing media has not been observed at the lower temperature of 65 °C, Mn and Co reveal to be strongly affected by the presence of a reductant agent. The similar faster kinetics and the higher extraction level of Co and Mn have also been observed in the literature due to the presence of sulfur dioxide [37]. This was attributed to higher potential difference in the reductive dissolution of MnO_2 ($MnO_2/S \Rightarrow \Delta E^o = 0.729$ V; $MnO_2/SO_{2(aq)} \Rightarrow \Delta E^o = 1.059$ V) compared to FeOOH (FeOOH/S ⇒ $\Delta E^o = 0.215$ V; $FeOOH/SO_{2(aq)} \Rightarrow \Delta E^o = 0.545$ V) [14]. Besides, Co and Mn-goethite have lower activation energy (< 75 kJ mol^{-1}) for acid dissolution [33].

It is worthy of note that heat was found to promote a more significant effect on AAL than RAAL. This may be due to (1) the favored decomposition of thiosulfate into sulfur and sulfur dioxide, both of which are intermediate reagents responsible for the pyrolusite and goethite reduction, and (2) the preferable dissolution of Mn oxide to goethite which is promoted at higher temperatures [14, 38].

The behavior observed in the leaching of Ni, Fe, and Mg suggests an association of these elements in the structure of goethite and chlorite phases that were identified as Ni-bearing minerals in the ore characterization. Extraction of Mn and Co

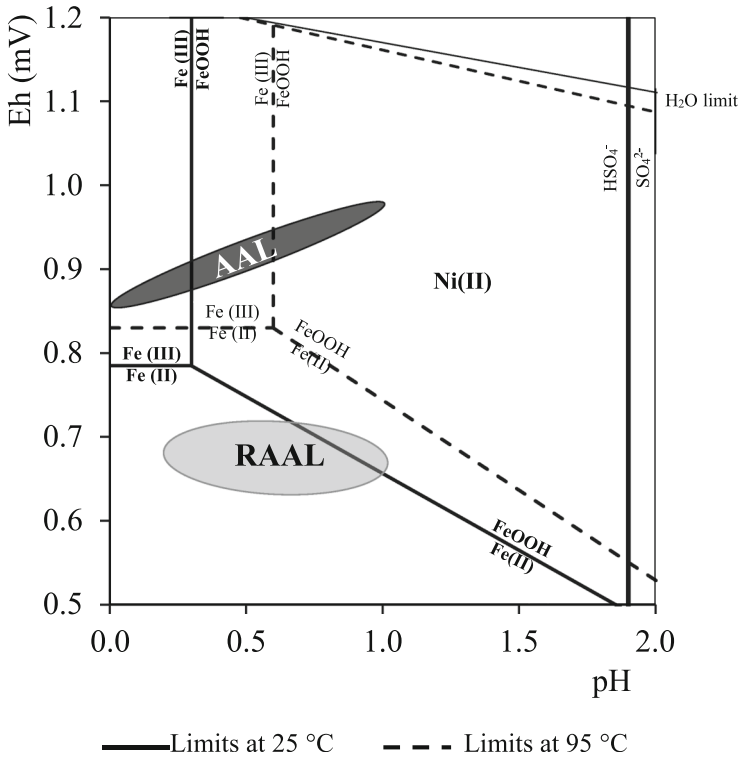

Fig. 10 Pourbaix diagram of Fe-H_2O, Ni-H_2O, and S-H_2O system at 25 and at 95 °C built with HSC© v.6.0. The input Fe, Ni, and S molalities are 0.712 mol kg^{-1}, 0.373 mol kg^{-1}, and 2.0 mol kg^{-1}, respectively

Table 4 Kinetic apparent constant of the shrinking core model for AAL

Element	Volume diffusion				Porous layer diffusion				Chemical reaction			
	0–15 min		15–120 min		0–15 min		15–120 min		0–15 min		15–120 min	
	k	R^2	K	R^2	k	R^2	k	R^2	k	R^2	k	R^2
AAL, without restoration												
Ni	0.0233	*0.7424*	0.0020	*0.9154*	0.0027	*0.9502*	0.0009	*0.9693*	0.0087	*0.7726*	0.0010	*0.9378*
Fe	0.0175	*0.8489*	0.0022	*0.9501*	0.0015	*0.9971*	0.0008	*0.9804*	0.0063	*0.8698*	0.0010	*0.9632*
Mg	0.0320	*0.6287*	0.0014	*0.9079*	0.0034	*0.8387*	0.0007	*0.9338*	0.0125	*0.6657*	0.0007	*0.9204*
Co	0.0259	*0.6861*	0.0017	*0.9185*	0.0034	*0.9016*	0.0008	*0.9490*	0.0095	*0.7181*	0.0008	*0.9322*
Mn	0.2510	*0.7453*	0.0028	*0.9798*	0.0031	*0.9537*	0.0016	*0.9791*	0.0095	*0.7784*	0.0015	*0.9845*
AAL, with restoration												
Ni	0.0249	*0.7656*	0.0023	*0.9574*	0.0031	*0.9671*	0.0011	*0.9933*	0.0094	*0.7987*	0.0012	*0.9749*
Fe	0.0221	*0.8566*	0.0021	*0.9237*	0.0024	*0.9989*	0.0009	*0.9740*	0.0082	*0.8836*	0.0010	*0.9439*
Mg	0.0399	*0.7973*	0.0021	*0.9780*	0.0091	*0.9909*	0.0019	*0.9892*	0.0166	*0.8595*	0.0015	*0.9867*
Co	0.0264	*0.8864*	0.0020	*0.9828*	0.0036	*0.9994*	0.0010	*0.9990*	0.0101	*0.9172*	0.0011	*0.9917*
Mn	0.0314	*0.8003*	0.0029	*0.9380*	0.0052	*0.9878*	0.0021	*0.9813*	0.0123	*0.8448*	0.0018	*0.9646*

Temperature: 95 °C. Solid-liquid ratio: 15%. Particle size fraction: − 75 μm. H_2SO_4: 2 mol L^{-1}. Stirring rate: 400 rpm

presented the same trend since these elements are probably associated within a standard structure or because they both partially substitute Fe in goethite, or may also be found in the structure of pyrolusite [3, 14, 25, 39].

3.4 Kinetic of Leaching of the Limiting Ore Fraction

The shrinking core model was not able to describe the experimental results depicted in Figs. 8 and 9. This means that there is not only one stage in the process for the − 75 μm fractions in the whole leaching period. Therefore, as reported in previous works [10, 40], the experimental results were split into two regions, 0–15 min and 15–120 min for individual evaluation. The time of 15 min was chosen based on the fast dissolution observed in the present work. MacCarthy et al. and Senanayake et al. have indicated that a change in the kinetics of leaching from laterite ores occurs due to distinct particle characteristics that cause different dissolution rates of phases [10, 11, 40, 41].

Table 5 Kinetic apparent constant of the shrinking core model for RAAL

Element	Volume diffusion				Porous layer diffusion				Chemical reaction			
	0–15 min		15–120 min		0–15 min		15–120 min		0–15 min		15–120 min	
	k	R^2	K	R^2	k	R^2	k	R^2	k	R^2	k	R^2
RAAL, without restoration												
Ni	0.0235	*0.8982*	0.0020	*0.9539*	0.0028	*0.9984*	0.0009	*0.9804*	0.0088	*0.9240*	0.0010	*0.9650*
Fe	0.0314	*0.5155*	0.0019	*0.9823*	0.0051	*0.6467*	0.0010	*0.9742*	0.0123	*0.5361*	0.0010	*0.9802*
Mg	0.0368	*0.6532*	0.0012	*0.9087*	0.0074	*0.8776*	0.0007	*0.9307*	0.0149	*0.7019*	0.0006	*0.9191*
Co	0.0416	*0.4928*	0.0003	*0.8945*	0.0097	*0.6121*	0.0002	*0.8998*	0.0174	*0.5191*	0.0002	*0.8970*
Mn	0.0368	*0.4405*	0.0016	*0.8929*	0.0072	*0.4926*	0.0011	*0.9387*	0.1480	*0.4502*	0.0010	*0.9165*
RAAL, with restoration												
Ni	0.0259	*0.6941*	0.0019	*0.8373*	0.0033	*0.9097*	0.0008	*0.8662*	0.0098	*0.7264*	0.0009	*0.8484*
Fe	0.0210	*0.9530*	0.0022	*0.8711*	0.0023	*0.9811*	0.0009	*0.9117*	0.0078	*0.9687*	0,0001	*0.8861*
Mg	0.0325	*0.4838*	0.0012	*0.8166*	0.0055	*0.5837*	0.0006	*0.8675*	0.0128	*0.4999*	0.0007	*0.8379*
Co	0.0369	*0.4745*	0.0009	*0.8604*	0.0073	*0.5678*	0.0005	*0.8920*	0.0149	*0.4920*	0.0005	*0.8745*
Mn	0.0480	*0.4977*	0.0010	*0.9385*	0.0137	*0.6320*	0.0009	*0.9631*	0.0210	*0.5339*	0.0007	*0.9546*

Temperature: 95 °C. Solid-liquid ratio: 15%. Particle size fraction: − 75 μm. H_2SO_4: 2 mol L^{-1}. Thiosulfate: 10 g L^{-1}. Stirring rate: 400 rpm

Tables 4 and 5 present the kinetic evaluation considering the two regimes of extraction versus time. The leaching control by volume diffusion mechanism was excluded due to a poorer data fit. In general, for the system with and without leaching solution restoration, it can be observed that the model considering porous layer diffusion control better represents the Ni, Fe, Mg, Co, and Mn data for both time regimes. Data from experiments with restoration exhibited a better fit due to the more accurate control of E_h and pH during the leaching.

Knowing that the porous layer diffusion controls the leaching process, the overall apparent kinetic constant order of $k_{Fe}<k_{Ni}<k_{Mn}<k_{Co}<k_{Mg}$ for AAL was observed. For RAAL, the order $k_{Fe}<k_{Ni}<k_{Mg}\cong k_{Co}<k_{Mn}$ was obtained. The higher kinetic constants for Co and Mn suggest that, even when it is in low grade in the ore, they are readily leached. The lower kinetic constant for Fe and Ni confirms that they are mainly present in refractory minerals, which require severe conditions for dissolution. This justifies the approach of assigning material of − 75 μm as a limiting leaching fraction.

4 Conclusions

In this work, a Brazilian ore composed of quartz, chlorite/lizardite, hematite, goethite, magnetite/maghemite, and chromite was investigated. Chlorite/lizardite and goethite were the main nickel-bearing minerals that exhibited high extractions for the coarser fraction (− 500 + 150 μm with 1.27% Ni) due to the major presence of silicates. The behavior of the lateritic nickel ore under leaching depends on its mineralogy and associated particle size. The fraction − 75 μm (64% of the ore) containing 2.06 % Ni and 49% of goethite was identified as the limiting fraction, thus requiring more extreme leaching conditions to provide appropriate extraction levels.

The use of reducing media at a solid-liquid ratio of 15%, 2 mol L^{-1} of H_2SO_4, and a stirring rate 400 rpm improved the extraction of metals for the limiting fraction, especially in the presence of thiosulfate. This reducing reagent presented better selectivity, safer operational conditions, and required lower dosage to allow extractions of 55% (Ni), 61% (Fe), 62% (Mg), 53% (Co), and 62% (Mn) at 95 °C. However, this low extraction obtained for Ni (50–60%) and also the similar level of impurities extracted (Mg, Mn, Co, Fe), may represent an economical and technological challenge in the downstream process. Additionally, the separation of Fe oxyhydroxide and Ni-bearing silicates minerals before leaching should be evaluated.

Control of E_h and pH by the restoration of the leaching solution did not provide the expected results in RAAL. However, for the AAL extraction, the data showed a slightly higher efficiency using solution restoration.

In most cases, it was observed that an increase in temperature increased the extraction of metals. This is except for Co and Mn in the RAAL, where the maximum extraction was obtained at a lower temperature of 65 °C. However, for Fe, an increase in temperature increased its extraction and the extraction of the associated Ni.

The kinetics of AAL and RAAL was found to be controlled by the porous layer diffusion mechanism in the two regions of time studied (0–15 min and 15–120 min). However, chemical control also presented a relatively good fit for the 15–120 min range, thus suggesting a mixed control.

Acknowledgments The authors wish to thank Brazilian research agencies FAPEMIG (Fundação de Amparo à Pesquisa do Estado de Minas Gerais), CAPES (Coordenação de Aperfeiçoamento de Pessoal de Nível Superior) and CNPq (Conselho Nacional de Desenvolvimento Científico e Tecnológico, Project Number 308044/2018-5) for financial support. The authors are also thankful to Vale Institute of Technology, and to Centro de Microscopia of Universidade Federal de Minas Gerais for analysis supports.

Compliance with Ethical Standards

Conflict of Interest The authors declare that they have no conflict of interest.

References

1. Survey USG (2020) Mineral commodity summaries 2020. U.S. Geological Survey. doi:https://doi.org/10.3133/mcs2020
2. Norgate T, Jahanshahi S (2010) Low grade ores—smelt, leach or concentrate? Miner Eng 23(2):65–73. https://doi.org/10.1016/j.mineng.2009.10.002
3. Andersen JCØ, Rollinson GK, Snook B, Herrington R, Fairhurst RJ (2009) Use of QEMSCAN® for the characterization of Ni-rich and Ni-poor goethite in laterite ores. Miner Eng 22(13):1119–1129. https://doi.org/10.1016/j.mineng.2009.03.012
4. Farrokhpay S, Filippov L (2016) Challenges in processing nickel laterite ores by flotation. Int J Miner Process 151:59–67. https://doi.org/10.1016/j.minpro.2016.04.007
5. Mohammadreza F, Mohammad N, Ziaeddin SS (2014) Nickel extraction from low grade laterite by agitation leaching at atmospheric pressure. Int J Min Sci Technol 24(4):543–548. https://doi.org/10.1016/j.ijmst.2014.05.019
6. Quast K, Connor JN, Skinner W, Robinson DJ, Addai-Mensah J (2015) Preconcentration strategies in the processing of nickel laterite ores Part 1: Literature review. Miner Eng 79:261–268. https://doi.org/10.1016/j.mineng.2015.03.017
7. Elias M (2002) Nickel laterite deposits—geological overview, resources and exploitation. Giant Ore Depositis: Charact Gen Explor: CODES Spec Publ 4(CODES Special Publication 4):205–220
8. Canterford J (1978) Leaching of some Australian nickeliferous laterites with sulphuric acid at atmospheric pressure. Proceedings of the Australasian Institute of Mining and Metallurgy (265):19-26
9. McDonald RG, Whittington BI (2008) Atmospheric acid leaching of nickel laterites review. Hydrometallurgy 91(1-4):35–55. https://doi.org/10.1016/j.hydromet.2007.11.009
10. MacCarthy J, Nosrati A, Skinner W, Addai-Mensah J (2015) Acid leaching and rheological behaviour of a siliceous goethitic nickel

laterite ore: Influence of particle size and temperature. Miner Eng 77:52–63. https://doi.org/10.1016/j.mineng.2014.12.031
11. MacCarthy J, Nosrati A, Skinner W, Addai-Mensah J (2016) Atmospheric acid leaching mechanisms and kinetics and rheological studies of a low grade saprolitic nickel laterite ore. Hydrometallurgy 160:26–37. https://doi.org/10.1016/j.hydromet.2015.11.004
12. Panda L, Rao DS, Mishra BK, Das B (2014) Characterization and dissolution of low-grade ferruginous nickel lateritic ore by sulfuric acid. Miner Metall Process 31(1):57–65. https://doi.org/10.1007/bf03402349
13. Das GK, de Lange JAB (2011) Reductive atmospheric acid leaching of West Australian smectitic nickel laterite in the presence of sulphur dioxide and copper(II). Hydrometallurgy 105(3-4):264–269. https://doi.org/10.1016/j.hydromet.2010.10.016
14. Li G, Rao M, Jiang T, Huang Q, Peng Z (2011) Leaching of limonitic laterite ore by acidic thiosulfate solution. Miner Eng 24(8):859–863. https://doi.org/10.1016/j.mineng.2011.03.010
15. Liu K, Chen Q, Hu H (2009) Comparative leaching of minerals by sulphuric acid in a Chinese ferruginous nickel laterite ore. Hydrometallurgy 98(3-4):281–286. https://doi.org/10.1016/j.hydromet.2009.05.015
16. Luo W, Feng Q, Ou L, Zhang G, Lu Y (2009) Fast dissolution of nickel from a lizardite-rich saprolitic laterite by sulphuric acid at atmospheric pressure. Hydrometallurgy 96(1-2):171–175. https://doi.org/10.1016/j.hydromet.2008.08.001
17. Thubakgale CK, Mbaya RKK, Kabongo K (2013) A study of atmospheric acid leaching of a South African nickel laterite. Miner Eng 54:79–81. https://doi.org/10.1016/j.mineng.2013.04.006
18. Luo J, Li G, Rao M, Peng Z, Zhang Y, Jiang T (2015) Atmospheric leaching characteristics of nickel and iron in limonitic laterite with sulfuric acid in the presence of sodium sulfite. Miner Eng 78:38–44. https://doi.org/10.1016/j.mineng.2015.03.030
19. Levenspiel O (2006) Chemical Reaction Engineering. 3rd edn. Wiley India Pvt. Limited
20. Fan R, Gerson AR (2013) Mineralogical characterisation of Indonesian laterites prior to and post atmospheric leaching. Hydrometallurgy 134-135:102–109. https://doi.org/10.1016/j.hydromet.2013.02.004
21. Pickles CA (2004) Microwave heating behaviour of nickeliferous limonitic laterite ores. Miner Eng 17(6):775–784. https://doi.org/10.1016/j.mineng.2004.01.007
22. Watling HR, Elliot AD, Fletcher HM, Robinson DJ, Sully DM (2011) Ore mineralogy of nickel laterites: controls on processing characteristics under simulated heap-leach conditions. Aust J Earth Sci 58(7):725–744. https://doi.org/10.1080/08120099.2011.602986
23. Astuti WHT, Sasaki K, Okibe N (2015) Kinetics of nickel extraction from Indonesian saprolitic ore by citric acid leaching under atmospheric pressure. Miner Metall Process 32(3):176–185. https://doi.org/10.1007/BF03402286
24. Carvalho e Silva MLRYR, Tolentino HCN, Enzeweiler J, Netto SM, Alves MCM (2003) Incorporation of Ni into natural goethite an investigation by X-ray adsorption spectroscopy. Am Mineral 88:876–882. https://doi.org/10.2138/am-2003-5-617
25. Manceau A, Schlegel ML, Musso M, Sole VA, Gauthier C, Petit PE, Trolard F (2000) Crystal chemistry of trace elements in natural and synthetic goethite. Geochim Cosmochim Acta 64(21):3643–3661. https://doi.org/10.1016/S0016-7037(00)00427-0
26. Puron AR (2001) Evidencias a favor de que la goethita es la principal portadora de niquel en los horizontes lateriticos de las cortezas ferroniqueliferas. Miner Geol 18(3-4):21–31
27. Hunter HMA, Herrington RJ, Oxley EA (2013) Examining Ni-laterite leach mineralogy & chemistry – a holistic multi-scale approach. Miner Eng 54:100–109. https://doi.org/10.1016/j.mineng.2013.05.002
28. Ferron C, Henry P (2008) The use of ferrous sulphate to enhance the dissolution of cobaltic minerals. Presentation at Hydrometallurgy
29. Senanayake G, Childs J, Akerstrom BD, Pugaev D (2011) Reductive acid leaching of laterite and metal oxides—a review with new data for Fe(Ni,Co)OOH and a limonitic ore. Hydrometallurgy 110(1-4):13–32. https://doi.org/10.1016/j.hydromet.2011.07.011
30. Cornell R, Posner A, Quirk J (1974) Crystal morphology and the dissolution of goethite. J Inorg Nucl Chem 36(9):1937–1946. https://doi.org/10.1016/0022-1902(74)80705-0
31. Chander S (1982) Atmospheric pressure leaching of nickeliferous laterites in acidic media. Trans Indian Inst Metals 35:365–371
32. Sidhu P, Gilkes R, Cornell R, Posner A, Quirk J (1981) Dissolution of iron oxides and oxyhydroxides in hydrochloric and perchloric acids. Clay Clay Miner 29(4):269–276. https://doi.org/10.1346/CCMN.1981.0290404
33. Lim-Nunez R, Gilkes R (1987) Acid dissolution of synthetic metalcontaining goethites and hematites. In: Schultz L, van Olphen H, Mumpton F (eds) Proceedings of the International Clay Conference. The Clay Minerals Society, Denver, USA, pp 197–204
34. Senanayake G, Das G (2004) A comparative study of leaching kinetics of limonitic laterite and synthetic iron oxides in sulfuric acid containing sulfur dioxide. Hydrometallurgy 72(1-2):59–72. https://doi.org/10.1016/S0304-386X(03)00132-4
35. Rice N, Strong L (1974) The leaching of lateritic nickel ores in hydrochloric acid. Can Metall Q 13(3):485–493. https://doi.org/10.1179/cmq.1974.13.3.485
36. Senanayake G (2003) A surface reaction kinetic model to compare the reductive leaching of iron from goethite, magnetite, and limonitic nickel laterite ores by acidic sulfur dioxide. Metall Mater Trans B 34(5):735–738. https://doi.org/10.1007/s11663-003-0043-8
37. Das G, Muir D, Senanayake G, Singh P, Hefter G (1997) Acid leaching of nickel laterites in the presence of sulphur dioxide at atmospheric pressure. Paper presented at the Hydrometallurgy and Refining of Nickel and Cobalt, Montreal, QC Canada, August 17-20
38. Kerker M (1951) The acid decomposition os sodium thiosulfate. J Chem Phys 19:1324–1325
39. Quaicoe I, Nosrati A, Skinner W, Addai-Mensah J (2014) Agglomeration and column leaching behaviour of goethitic and saprolitic nickel laterite ores. Miner Eng 65:1–8. https://doi.org/10.1016/j.mineng.2014.04.001
40. Liu K, Chen Q, Yin Z, Hu H, Ding Z (2012) Kinetics of leaching of a Chinese laterite containing maghemite and magnetite in sulfuric acid solutions. Hydrometallurgy 125-126:125–136. https://doi.org/10.1016/j.hydromet.2012.06.001
41. Senanayake G, Das GK, de Lange A, Li J, Robinson DJ (2015) Reductive atmospheric acid leaching of lateritic smectite/nontronite ores in H2SO4/Cu(II)/SO2 solutions. Hydrometallurgy 152:44–54. https://doi.org/10.1016/j.hydromet.2014.12.001